Electrocatalysis

DOI: 10.1002/ange.201304658

Biomimetic Synthesis of an Ultrathin Platinum Nanowire Network with a High Twin Density for Enhanced Electrocatalytic Activity and Durability**

*Lingyan Ruan, Enbo Zhu, Yu Chen, Zhaoyang Lin, Xiaoqing Huang, Xiangfeng Duan, and Yu Huang**

Fuel cells have attracted much research interest as they are promising candidates for providing clean energy.[1] A fuel cell catalyzes reactions between a fuel (e.g., hydrogen or alcohols) at the anode and the oxidant (molecular oxygen) at the cathode, converting chemical energy into electrical power.[1] One of the most critical challenges for fuel-cell applications is the sluggish reduction kinetics of the oxygen reduction reaction (ORR) at the cathode.[1] So far, platinum and Pt-based nanomaterials are recognized as the most effective electrocatalysts for the ORR.[1,2] Current state-of-the-art electrocatalysts rely almost exclusively on Pt black or Pt nanoparticles (2–5 nm) dispersed onto a carbon black support (Pt/C).[1,2] However, the practical large-scale commercialization of fuel cells is still a great challenge because of the loss of electrochemical surface area (ECSA) and the decrease of catalytic activity over time.[3,4] Another important issue of fuel-cell applications is the anodic reaction, that is, the oxidation of hydrogen or alcohols (for example, methanol or ethanol).[1] The direct methanol fuel cell is particularly attractive due to its high volumetric energy density and its ease of storage and transport compared to the hydrogen fuel cell.[5] Similar to the cathode, Pt-based nanomaterials are currently used as the most efficient electrocatalysts for the methanol oxidation reaction (MOR), which unfortunately suffers from the same problems including poor reaction kinetics and poisoning.[5–7] Therefore, the development of electrocatalysts with improved catalytic activity and durability is highly desirable but remains a significant challenge.

The control on nanomaterial structures provides a sensitive knob to tune the properties and improve the functions.[8,9] Nanostructured Pt with various morphologies has been extensively exploited in the search to improve the electrocatalytic performance.[10–14] To this end, one-dimensional (1D) nanostructures, such as nanowires, represent an important research direction because 1D nanostructures possess unique advantages compared to their zero-dimensional (0D) counterparts. For example, the structural anisotropy can slow down the ripening process; and the display of long segments of low-index crystalline planes along the nanowire is particularly beneficial for the ORR.[5,15,16] As a result, various methods including both top-down and bottom-up have been developed to synthesize Pt 1D nanostructures.[17–25] Most prior studies reported the production of single-crystalline Pt nanowires.[18,21,23–25] Meanwhile, twinning of materials has been shown to greatly affect the physical and chemical material properties, including various surface adsorption, heterogeneous catalytic, and electrocatalytic processes.[26–29] While nanotwins have been widely employed to enhance mechanical properties, very limited effort has been devoted to engineering of twin defects in nanomaterials for improved catalysis and electrocatalysis.[30,31]

Herein, we report an ultrathin Pt multiple-twinned nanowire network (MTNN) as an efficient electrocatalyst, which exhibits a higher ECSA and much improved activity toward both ORR and MOR when compared to current state-of-the-art commercial Pt/C electrocatalysts. Furthermore, it shows significantly improved durability with much less decay of ECSA at prolonged reaction times. The unique feature of the nanowire in our studies is its high density of twin planes, which have been proposed to play a significant role in the promotion of the electrocatalytic performance.[28,29]

The Pt MTNN was synthesized by biomimetic synthesis using a specific Pt-binding peptide (amino acid sequence Ac-TLHVSSY-$CONH_2$, named BP7A, identified through phage display).[32,33] Peptide-directed biomimetic syntheses have emerged as a new synthetic route and demonstrated the potential to maneuver nanomaterial structures and functions in a controllable manner under mild environmental-benign conditions.[34–38] Particularly, peptide BP7A has been demonstrated to lead to exclusive formation of twinned Pt nanoparticles, which is uncommon in conventional syntheses.[38] Here, we further exploit its potential for the synthesis of 1D Pt nanowire with dense twin defects. Although nanowires with twin defects have been observed before, the occurrence of twinning appeared relatively random and rare.[18–25] This is the first report on synthesis of Pt nanowires that are ultrathin yet show a high twin population.

The synthesis was carried out at room temperature in aqueous solution using the peptide BP7A as the surfactant

[*] L. Ruan, E. Zhu, Y. Chen, X. Huang, Prof. Y. Huang
Department of Materials Science and Engineering
University of California, Los Angeles
Los Angeles, CA 90095 (USA)
E-mail: yhuang@seas.ucla.edu
Z. Lin, Prof. X. Duan
Department of Chemistry and Biochemistry
University of California, Los Angeles
Los Angeles, CA 90095 (USA)

[**] We acknowledge the support from ARO (award number 54709-MS-PCS) and ONR (award number N00014-08-1-0985). We thank EICN at CNSI for the TEM support. Y.H. acknowledges the support from a Sloan Research Fellowship.

Supporting information for this article is available on the WWW under http://dx.doi.org/10.1002/anie.201304658.

molecule. The Pt precursor H_2PtCl_6 (1 mM) was first mixed with the peptide in solution (100 μg mL^{-1}), followed by introduction of reducing agents ascorbic acid (5 mM) and sodium borohydride (0.8 mM). Then, more Pt precursor K_2PtCl_4 (0.5 mM) was added after sodium borohydride to sustain complete growth of the nanowire (see the Supporting Information for experimental details). The as-synthesized Pt MTNN is shown in Figure 1 A and B. The low-magnification TEM image (Figure 1 A) shows the abundant wavy Pt nanowire is along ⟨111⟩, but it may change from one particular ⟨111⟩ direction to another < 111 > direction, as indicated by the white arrows in Figure 1 D,E,G. This change in growth direction contributes to the zigzag wavy morphology of the nanowire (Figure 1 D,E), and also to the branching of the nanowire (Figure 1 G). Twin defects were frequently observed cross-sectioning the nanowire, as indicated by the blue arrows (Figure 1 C,F), and also at joints where the nanowire changes growth direction (Figure 1 D). Along with twin defects, surface defects such as corner and edge atoms as well as high-index facets are observed along the nanowire, which would potentially contribute to the ORR activity.[39,40] The occurrence of abundant twinning may be the result of the attachment growth mode of the nanowire mediated by the peptide, which will be discussed in the following; and also comes from the specific stabilization of the peptide to twinning defects as previously reported.[38] More mechanistic studies regarding the stabilization of the peptide to twinning defects are under way. Despite its ultrathin and twin-rich nature, the crystallinity of Pt MTNN was confirmed by powder X-ray diffraction (Figure 1 H). Diffraction peaks were indexed to (111), (200), (220), and (311) reflections of face-centered cubic (fcc) Pt (JCPDS no. 87-0647). All diffraction peaks are broadened, indicating nanoscale structural features. In addition, energy-dispersive X-ray spectroscopy (EDS) was performed on a random selection of the sample, showing these Pt MTNNs are composed only of platinum (Figure 1 I). The Cu signals arise from the TEM grid.

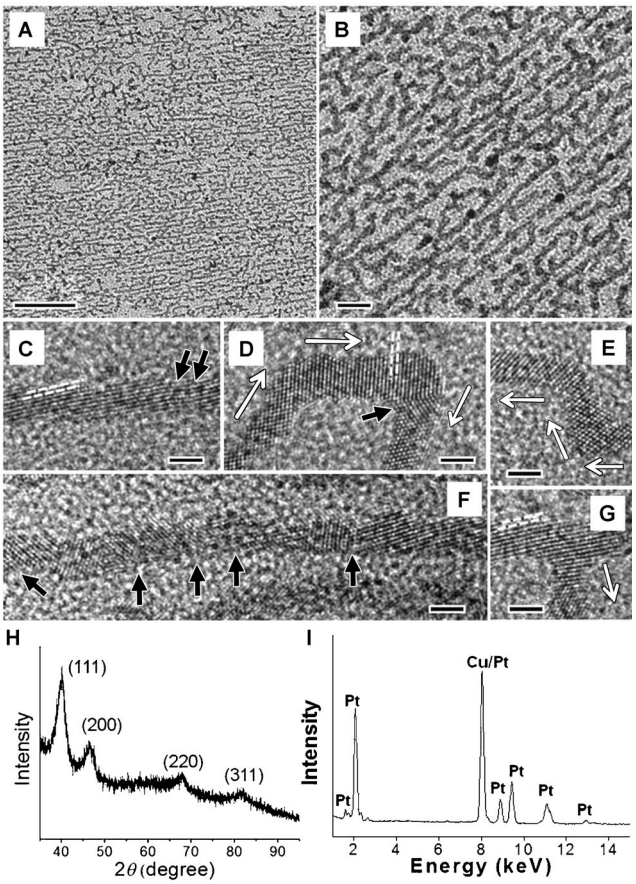

Figure 1. A and B) Low- and high-magnification TEM images of Pt MTNN. C–G) High-resolution TEM images of Pt MTNN. Black arrows indicate the presence of twin defects; whereas white arrows indicate the growth directions. H) X-ray diffractogram of Pt MTNN. I) EDX of Pt MTNN. The sale bares are 50 (A), 10 (B), and 2 nm (C–G). The interlayer distance given by dashed lines in (C, D, and G) is 0.23 nm.

wires interconnected with each other forming nanowire networks. The higher-magnification TEM image (Figure 1 B) shows an individual nanowire with a thin diameter of about 2 nm. The structure of Pt MTNN was further characterized with high-resolution TEM (HRTEM, Figure 1 C–G). The measured lattice spacing of 0.23 nm is consistent with the {111} lattice plane of Pt. The nanowire shows relative long segments of crystal planes as compared to those ultrasmall Pt nanoparticles, and the majority of the displayed facets are low-index {111} planes (Figure 1 C), which have been shown to be more active towards the ORR than the {100} planes in acidic media.[39,40] The typical growth direction of the nano-

The dynamics of the Pt MTNN formation process was studied by TEM and HRTEM (Figure 2). Both small primary particles and short wires formed at the initial stage of the reaction (Figure 2 A). With increasing reaction time, network morphology started to appear (Figure 2 B). The width of nanowires changed very little throughout the growth process, suggesting that nanowires grow from primary nanoparticles

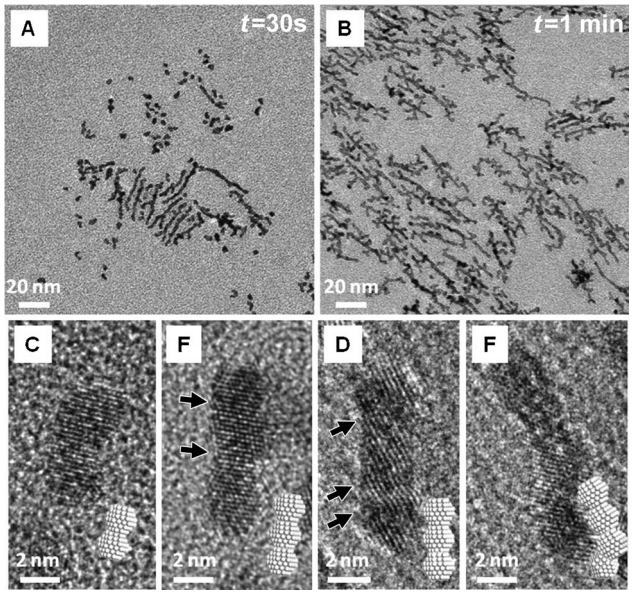

Figure 2. A and B) TEM images of Pt MTNN formed after 30 s and 1 minute, respectively. C–F) High-resolution TEM images of Pt MTNN formed after 30 s. Black arrows indicate presence of twin defects.

through oriented attachment.[41] Nanowires formed at the initial stage were closely examined under HRTEM (Figure 2C–F and Figure S1 in the Supporting Information). Figure 2C–F show various number (2-4) of primary nanoparticles attached together leading to lengthening of the nanowires. As indicated by the black arrows, twinning was already frequently observed in these initially formed short wires. Figure S1 shows in more detail the appearance of joint area between two primary particles, and a twin plane formed between two primary particles. Previous studies have suggested both lattice-matched and lattice-mismatched attachment modes in nanowire growth, with the lattice-matched attachment leading to a single-crystal structure and the lattice-mismatched attachment leading to twin planes in the wire.[42] Also, reconstruction and rearrangement during the growth process would results in the disappearance of twin defects.[42] The abundance of twin defects observed in the final product suggests lattice-mismatched attachment is enhanced and preserved with the existence of peptide molecule, possibly due to the specific stabilization of twin sites by the BP7A peptides.[38] The peptide concentration was also found to be a critical parameter in the formation of nanowires. Nanowires form at sufficient peptide concentration, while only nanoparticles form at lower peptide concentration (Figure S2). This may be attributed to stronger confinement on primary particles at higher peptide concentration, and stronger intermolecular interactions between peptides which drives the assembly process.[43]

With the unique structural features, Pt MTNN was evaluated as an electrocatalyst, and benchmarked against current state-of-the-art commercial Johnson Matthey (JM) Pt/C catalyst. Pt MTNN was loaded onto carbon black nanoparticles through a previously established process (Figure S3) and washed repeatedly before the measurement (see the Supporting Information for experimental details).[44] The electrocatalytic activity was first probed using cyclic voltammetry (CV) recorded at room temperature in a nitrogen-purged 0.1 M $HClO_4$ solution at a sweep rate of 50 $mV s^{-1}$ (Figure 3A). CV curves show typical peaks associated with hydrogen adsorption/desorption (Figure 3A).[11] The ECSA was calculated by measuring the charge associated with hydrogen adsorption/desorption between 0 and 0.4 V and assuming $Q_{ref} = 0.21\ mC cm^{-2}$ for the adsorption of a hydrogen monolayer. Notably, Pt MTNN showed an even higher specific ECSA ($80.36\ m^2 g^{-1}$) than the JM Pt/C catalyst ($77.77\ m^2 g^{-1}$). This may result from the ultrathin nature of the nanowires.

The ORR catalytic activity was tested using a rotating disk electrode (RDE) in an oxygen-saturated 0.1 M $HClO_4$ solution at a sweep rate of 10 $mV s^{-1}$ and at a rotation rate of 1600 rpm. The polarization curves show ORR onsets between 0.8 and 0.9 V (vs. the reversible hydrogen electrode, RHE) consistent with nanostructured platinum electrocatalysts (Figure S4).[11,15] Notably, Pt MTNN shows a slight shift toward higher potential compared with the JM Pt/C catalyst, suggesting a decrease in the ORR overpotential,[1] which can be attributed to the rich long segments of the {111} planes on the nanowire surface. The measured kinetic current density at 0.9 V was normalized over the Pt loading weight

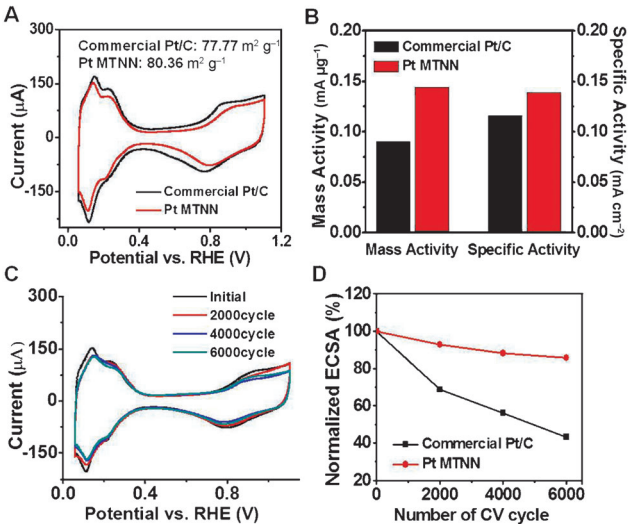

Figure 3. A) CV curves of the JM Pt/C and Pt MTNN catalysts in a deoxygenated 0.1 M $HClO_4$ solution at a scan rate of 50 $mV s^{-1}$. B) Corresponding mass activities and specific activities at 0.9 V of JM Pt/C and Pt MTNN, respectively. C) CV curves of Pt MTNN before and after an accelerated durability test (JM Pt/C is shown in the Supporting Information). The test was carried out at room temperature in an O_2-saturated 0.1 M $HClO_4$ solution with cyclic potentials sweeping between 0.6 and 1.1 V at a sweep rate of 50 $mV s^{-1}$. D) Loss of ECSA of JM Pt/C and Pt MTNN as a function of the cycling number.

and ECSA to yield the mass activity and specific activity, respectively (Figure 3B). Pt MTNN showed a mass activity of 0.144 $mA \mu g^{-1}$, a 58.2% increase compared with the JM Pt/C catalyst (0.091 $mA \mu g^{-1}$). Although with a higher ECSA, Pt MTNN still shows a higher specific activity (0.139 $mA \mu g^{-1}$) compared with the JM Pt/C catalyst (0.116 $mA \mu g^{-1}$). To further explore the kinetics of the ORR, we carried out a Koutecky–Levich (K-L) plot at various potentials (Figure S5). The kinetic current density versus rotation speed plotted at varying potentials all show a linear relationship with a consistent slope, suggesting that the ORR catalyzed by Pt MTNN closely follows the highly desirable $4e^-$ process.[15]

Since the decay of the electrocatalyst at the electrode remains an important issue for fuel-cell applications, we further examined the stability of Pt MTNN by an accelerated durability test (ADT). ADT was conducted at room temperature in O_2-saturated 0.1 M $HClO_4$ solutions by applying cyclic potential sweeps between 0.6 and 1.1 V versus RHE at a sweep rate of 50 $mV s^{-1}$ (Figure 3C,D). Pt MTNN showed excellent stability and a little drop of the ECSA during the test (Figure 3C), while JM Pt/C showed a much faster decrease of ESCA (Figure S6). The ECSA drops of Pt MTNN and JM Pt/C were normalized to their initial ECSA, respectively (Figure 3D). After 6000 cycles, Pt MTNN lost 14.2% of its initial ECSA, whereas the JM Pt/C catalyst suffered a severe degradation of 56.7% loss of its initial ECSA. We suggest the stability of the nanowires may come from its unique structure, that is, an ultrathin 1D structure which could slow down the ripening and dissolution process. Moreover, nanotwins have been observed to slow down the atomic transport process, which might also contribute to the overall stability of the nanowires.[31] The morphology changes

of Pt MTNN and JM Pt/C before and after ADT were investigated by TEM (Figure S7). The Pt nanoparticle size of the JM Pt/C catalyst increased from 2–5 nm to 5–25 nm, suggesting considerable nanoparticle ripening and aggregation. Although having some increase in diameter and becoming shorter, Pt MTNN remained its 1D morphology, and the twin planes remain frequently observed (Figure S8).

We further evaluated the electrocatalytic performance of Pt MTNN in MOR, using CV measurement recorded in 0.1 M H_2SO_4 electrolyte with 0.5 M methanol at a sweep rate of 50 mV s^{-1} (Figure 4 A). There are two oxidation peaks for

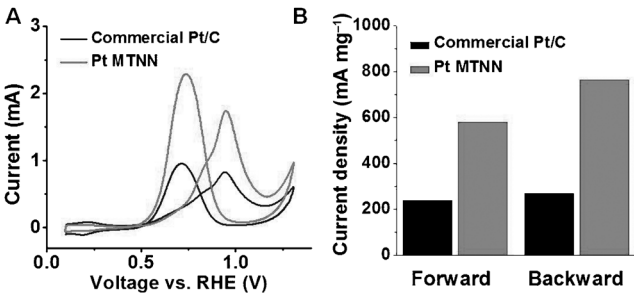

Figure 4. A) CV curves of JM Pt/C and Pt MTNN catalysts in a deoxygenated 0.5 M H_2SO_4 solution containing 1 M methanol at a scan rate of 50 mV s^{-1}. B) Corresponding mass activities of JM Pt/C and Pt MTNN.

methanol oxidation, that is, a 0.94 V peak (vs. RHE) in the anodic scan and a 0.7 V peak (vs. RHE) in the cathodic scan which is commonly assigned to the oxidation of partially oxidized species that adsorb onto the Pt surface after the anodic scan.[5] The current density can be directly related to the catalytic activity. As shown in Figure 4 A, the catalytic activity of Pt MTNN exceeds that of the JM Pt/C catalyst in both forward and backward scan. The forward-current peak density of Pt MTNN is 580.97 mA mg^{-1}, which is 148.5 % higher than that of the JM Pt/C catalyst (237.77 mA mg^{-1}). The backward peak current density is 764.04 mA mg^{-1}, which is 182.8 % higher than that of the JM Pt/C catalyst (270.19 mA mg^{-1}). Emergence of grain boundaries at the surface has been proposed to serve as active sites with greatly improved MOR activity.[28,29] The presence of high-density twin defects cross-sectioning the nanowire may create more surface-active sites and therefore facilitate the oxidation process.

In summary, we have developed a 1D Pt nanowire network structure with a high density of twin planes as an efficient electrocatalyst for fuel-cell applications. Our studies demonstrate that the nanostructure shows much enhanced activity in both ORR and MOR. Moreover, they show a greatly improved durability in the ORR at prolonged reaction times. The electrocatalytic performance improvement is attributed to the unique structure of the nanowire, that is, an ultrathin 1D morphology with a large population of twin planes. This unique structure demonstrates that engineering of structural defects can be used to design next-generation electrocatalysts. Moreover, defects have also been shown to have significant influence on many surface-sensitive catalysis processes, for example, defect sites have been found to greatly increase the catalytic activity in the reduction of nitrophenol or potassium ferricyanide.[45] More research effort could be devoted to defect engineering in the design of novel catalysts.[46] Taken together, our studies demonstrate control on the production of unique nanostructures and structure-enhanced properties, which is the focal point of designing nanomaterials for various applications.

Received: May 30, 2013
Published online: October 2, 2013

Keywords: electrocatalysis · nanowires · peptides · platinum · twin density

[1] K. Debe, *Nature* **2012**, *486*, 43 – 51.
[2] N. Tian, Z. Y. Zhou, S. G. Sun, *J. Phys. Chem. C* **2008**, *112*, 19801 – 19817.
[3] Y. Y. Shao, G. P. Yin, Y. Z. Gao, *J. Power Sources* **2007**, *171*, 558 – 566.
[4] A. Rabis, P. Rodriguez, T. J. Schmidt, *ACS Catal.* **2012**, *2*, 864 – 890.
[5] C. Koenigsmann, S. S. Wong, *Energy Environ. Sci.* **2011**, *4*, 1161 – 1176.
[6] X. W. Zhou, R. H. Zhang, Z.-Y. Zhou, S. G. Sun, *J. Power Sources* **2011**, *196*, 5844 – 5848.
[7] A. X. Yin, X. Q. Min, Y. W. Zhang, C. H. Yan, *J. Am. Chem. Soc.* **2011**, *133*, 3816 – 3819.
[8] J. Y. Chen, B. Lim, E. P. Lee, Y. N. Xia, *Nano Today* **2009**, *4*, 81 – 95.
[9] K. Zhou, Y. Li, *Angew. Chem.* **2012**, *124*, 622 – 635; *Angew. Chem. Int. Ed.* **2012**, *51*, 602 – 613.
[10] Z. M. Peng, H. Yang, *Nano Today* **2009**, *4*, 143 – 164.
[11] Y. H. Bing, H. S. Liu, L. Zhang, D. Ghosh, J. J. Zhang, *Chem. Soc. Rev.* **2010**, *39*, 2184 – 2202.
[12] X. Yu, D. Wang, Q. Peng, Y. Li, *Chem. Commun.* **2011**, *47*, 8094 – 8096.
[13] A. X. Yin, X. Q. Min, W. Zhu, H. S. Wu, Y. W. Zhang, C. H. Yan, *Chem. Commun.* **2012**, *48*, 543 – 545.
[14] S. Guo, S. Dong, E. Wang, *ACS Nano* **2010**, *4*, 547 – 555.
[15] C. Koenigsmann, M. E. Scofield, H. Q. Liu, S. S. Wong, *J. Phys. Chem. Lett.* **2012**, *3*, 3385 – 3398.
[16] S. H. Sun, G. X. Zhang, D. S. Geng, Y. G. Chen, R. Y. Li, M. Cai, X. L. Sun, *Angew. Chem.* **2011**, *123*, 442 – 446; *Angew. Chem. Int. Ed.* **2011**, *50*, 422 – 426.
[17] E. J. Menke, M. A. Thompson, C. Xiang, L. C. Yang, R. M. Penner, *Nat. Mater.* **2006**, *5*, 914 – 919.
[18] J. Y. Chen, T. Herricks, M. Geissler, Y. N. Xia, *J. Am. Chem. Soc.* **2004**, *126*, 10854 – 10855.
[19] X. W. Teng, W. Q. Han, W. Ku, M. Hucker, *Angew. Chem.* **2008**, *120*, 2085 – 2088; *Angew. Chem. Int. Ed.* **2008**, *47*, 2055 – 2058.
[20] Y. Song, R. M. Garcia, R. M. Dorin, H. R. Wang, Y. Qiu, E. N. Coker, W. A. Steen, J. E. Miller, J. A. Shelnutt, *Nano Lett.* **2007**, *7*, 3650 – 3655.
[21] L. G. Zhang, N. Li, F. M. Gao, L. Hou, Z. M. Xu, *J. Am. Chem. Soc.* **2012**, *134*, 11326 – 11329.
[22] L. Hu, X. Cao, L. Chen, J. Zheng, J. Lu, X. Sun, H. Gu, *Chem. Commun.* **2012**, *48*, 3445 – 3447.
[23] L. Hu, X. Cao, D. Ge, H. Hong, Z. Guo, L. Chen, X. Sun, J. Tang, J. Zheng, J. Lu, H. Gu, *Chem. Eur. J.* **2011**, *17*, 14283 – 14287.
[24] B. Y. Xia, W. T. Ng, H. B. Wu, X. Wang, X. W. Lou, *Angew. Chem.* **2012**, *124*, 7325 – 7328; *Angew. Chem. Int. Ed.* **2012**, *51*, 7213 – 7216.

[25] B. Y. Xia, H. B. Wu, Y. Yan, X. W. Lou, X. Wang, *J. Am. Chem. Soc.* **2013**, *135*, 9480 – 9485.
[26] K. D. Rendulic, A. Winkler, H. P. Steinruck, *Surf. Sci.* **1987**, *185*, 469 – 478.
[27] R. Vidruk, M. V. Landau, M. Herskowitz, M. Talianker, N. Frage, V. Ezersky, N. Froumin, *J. Catal.* **2009**, *263*, 196 – 204.
[28] N. P. Lebedeva, M. T. M. Koper, J. M. Feliu, R. A. van Santen, *J. Phys. Chem. B* **2002**, *106*, 12938 – 12947.
[29] O. V. Cherstiouk, A. N. Gavrilov, L. M. Plyasova, I. Y. Molina, G. A. Tsirlina, E. R. Savinova, *J. Solid State Electrochem.* **2008**, *12*, 497 – 509.
[30] Y. M. Wang, M. W. Chen, F. H. Zhou, E. Ma, *Nature* **2002**, *419*, 912 – 915.
[31] K. C. Chen, W. W. Wu, C. N. Liao, L. J. Chen, K. N. Tu, *Science* **2008**, *321*, 1066 – 1069.
[32] Y. J. Li, G. P. Whyburn, Y. Huang, *J. Am. Chem. Soc.* **2009**, *131*, 15998 – 15999.
[33] Y. J. Li, Y. Huang, *Adv. Mater.* **2010**, *22*, 1921 – 1925.
[34] M. B. Dickerson, K. H. Sandhage, R. R. Naik, *Chem. Rev.* **2008**, *108*, 4935 – 4978.
[35] C. Y. Chiu, L. Y. Ruan, Y. Huang, *Chem. Soc. Rev.* **2013**, *42*, 2512 – 2527.
[36] B. D. Briggs, M. R. Knecht, *J. Phys. Chem. Lett.* **2012**, *3*, 405 – 418.
[37] C. Y. Chiu, Y. J. Li, L. Y. Ruan, X. C. Ye, C. B. Murray, Y. Huang, *Nat. Chem.* **2011**, *3*, 393 – 399.
[38] L. Y. Ruan, C. Y. Chiu, Y. J. Li, Y. Huang, *Nano Lett.* **2011**, *11*, 3040 – 3046.
[39] N. M. Markovic, H. A. Gasteiger, P. N. Ross, *J. Phys. Chem.* **1995**, *99*, 3411 – 3415.
[40] N. M. Marković, T. J. Schmidt, V. Stamenkovic, P. N. Ross, *Fuel Cells* **2001**, *1*, 105 – 116.
[41] Z. M. Peng, H. J. You, H. Yang, *Acs Nano* **2010**, *4*, 1501 – 1510.
[42] J. M. Yuk, J. Park, P. Ercius, K. Kim, D. J. Hellebusch, M. F. Crommie, J. Y. Lee, A. Zettl, A. P. Alivisatos, *Science* **2012**, *336*, 61 – 64.
[43] B. Gao, G. Arya, A. R. Tao, *Nat. Nanotechnol.* **2012**, *7*, 433 – 437.
[44] Y. J. Li, Y. J. Li, E. B. Zhu, T. McLouth, C. Y. Chiu, X. Q. Huang, Y. Huang, *J. Am. Chem. Soc.* **2012**, *134*, 12326 – 12329.
[45] G. W. W. Qin, W. L. Pei, X. M. Ma, X. N. Xu, Y. P. Ren, W. Sun, L. Zuo, *J. Phys. Chem. C* **2010**, *114*, 6909 – 6913.
[46] I. Lee, M. A. Albiter, Q. Zhang, J. Ge, Y. Yin, F. Zaera, *Phys. Chem. Chem. Phys.* **2011**, *13*, 2449 – 2456.

